# Evidence for Periodic Variations in the Thickness of Saturn's Nightside Plasma Sheet

M. F. Thomsen[(1)], C. M. Jackman[(2)], S. W. H. Cowley[(3)], X. Jia[(4)], M. G. Kivelson[(4,5)], G. Provan[(3)]

[(1)] Planetary Science Institute, 1700 East Fort Lowell, Suite 106, Tucson, AZ, 85719, USA

[(2)] Department of Physics and Astronomy, University of Southampton, Southampton, SO17 1BJ, UK

[(3)] Department of Physics and Astronomy, University of Leicester, Leicester LE1 7RH, UK

[(4)] Climate and Space Sciences and Engineering, University of Michigan, Ann Arbor, MI, 48109, USA

[(5)] Earth Planetary and Space Sciences, University of California, Los Angeles, CA, 90095, USA

Abstract

During certain portions of the Cassini mission to Saturn, Cassini made repeated and periodic crossings of the magnetospheric current sheet that lies near the magnetic equator and extends well down the magnetospheric tail. These repeated crossings are part of the puzzling set of planetary period variations in numerous magnetospheric properties that

have been discovered at Saturn. During 2010 these periodic crossings often display asymmetries such that the northbound crossing occurs faster than the southbound crossing or vice versa, while at other times the crossings are more symmetric. The character of the crossings is well organized by the relative phase of the northern vs. southern perturbation currents inferred in earlier analyses of the magnetic field observations. Further, the dependence of the character of the crossings on the relative phase is consistent with similar asymmetries predicted both by the dual rotating current systems inferred from magnetic field observations and by global MHD models that incorporate the effects of hypothesized atmospheric vortices. The two models are themselves in generally good agreement on those predictions. In both models the asymmetries are attributable to a periodic thickening and thinning of the magnetospheric current sheet, combined with a periodic vertical flapping of the sheet. The Cassini observations thus provide additional observational support to such current systems as a likely explanation for many of the known magnetospheric planetary period variations.

## Introduction

Saturn's magnetosphere has now been visited by four spacecraft (Pioneer 11, Voyagers 1 and 2, and Cassini) and remotely observed by the Ulysses radio wave experiment. One of the most puzzling discoveries from these missions has been the occurrence of periodic variations in a wide range of magnetospheric observables, from bursts of Saturn Kilometric Radiation (SKR) [e.g., Warwick et al., 1981; Desch and Kaiser, 1981; Galopeau and Lecacheux, 2000; Gurnett et al., 2009; Lamy, 2011] to in situ magnetic field [e.g., Espinosa and Dougherty, 2000; Cowley et al., 2006; Southwood and

47 Kivelson, 2007; Andrews et al., 2008], energetic particle [e.g., Carbary and Krimigis,
48 1982; Carbary et al., 2007, 2008], and plasma [e.g., Burch et al., 2009; Arridge et al.,
49 2011; Nemeth et al., 2016] properties. These periodicities occur at approximately the
50 planetary rotation rate, which is inferred from tracking identifiable cloud features in the
51 atmosphere since at Saturn it is not possible to observe a solid planetary body. When they
52 were first observed, the periodicity of the SKR bursts was taken to be the best
53 determination of the planetary spin period.

54 The initial puzzling aspect of these periodicities was their very existence since
55 Saturn's magnetic dipole is very nearly aligned with its rotational axis, with no tilt or
56 offset to break the cylindrical symmetry. Further confounding the mystery was the
57 discovery that the SKR period actually varied slowly in time [e.g., Galopeau and
58 Lecacheux, 2000], clearly incompatible with a signature of underlying planetary rotation.
59 Moreover, evidence was then found for not just the one but two different periodicities,
60 one associated with SKR and magnetic field variations in the northern hemisphere and
61 the other associated with the southern hemisphere [e.g., Galopeau and Lecacheux, 2000;
62 Kurth et al., 2008; Gurnett et al., 2009]. These findings were reviewed by Carbary and
63 Mitchell [2013] and have subsequently been supplemented by a number of studies, many
64 of which are summarized by Cowley et al. [2016a].

65 These observations have given rise to a large number of hypothesized sources of
66 the periodicities [e.g., Espinosa et al., 2003; Gurnett et al., 2007; Goldreich and Farmer,
67 2007; Carbary et al., 2007; Southwood and Kivelson, 2007; Mitchell et al., 2009a;
68 Khurana et al., 2009; Burch et al., 2009; Brandt et al., 2010; for reviews see Mitchell et
69 al., 2009b, and Carbary and Mitchell, 2013]. Two of the models that have been

particularly successful in reproducing a wide range of observed periodic features are the empirical dual rotating current system (which we will refer to as DRC henceforth) [e.g., Southwood and Kivelson, 2007; Andrews et al., 2010, 2012; Provan et al., 2012; Cowley et al., 2016b] and the atmospheric vortex model (referred to as AV) [Jia et al., 2012; Jia and Kivelson, 2012]. These two models are closely related: The former is based on an analytical description of the periodic magnetic field perturbations, and the latter is based on a global magnetospheric MHD model that imposes in the ionosphere a rotating pattern of flow designed to drive the field-aligned currents [recently discussed by Hunt et al., 2014 and Southwood and Cowley, 2014] needed to account for the very same periodic magnetic field fluctuations. Both models predict periodic variations in the field and plasma properties throughout the magnetosphere, rather successfully explaining many of the observed periodicities. Two further advantages of these two models over many of the other proposed periodicity-producing mechanisms are that they provide natural explanations of how the phase of the periodic variations can remain constant over many months or years, and they naturally allow for dual periodicities and slow temporal variations in the periods.

Of particular interest for the present study, both these models predict periodic vertical motions of the magnetospheric current sheet (accounting for the periodic current sheet encounters commonly seen with the Cassini spacecraft) and periodic thickening and thinning of the current sheet [e.g., Jia and Kivelson, 2012; Provan et al., 2012; Cowley et al., 2016b]. Such modulation of the current sheet thickness has previously been inferred from Cassini observations [e.g., Morooka et al., 2009; Provan et al., 2012]. In the present work, we show observations of asymmetries in the north-to-south and south-to-north

93 crossings of the tail current sheet that provide additional evidence for periodic
94 modulation of the current sheet thickness. Further, we show that the nature of the
95 asymmetries depends on the relative phase of the north and south current systems in a
96 manner that is consistent with the expectations of both the DRC and AV models
97 mentioned above.
98
99 Observations
100 We report observations from the Cassini magnetometer (MAG) [Dougherty et al.,
101 2004] obtained during 2010, a time of repeated low-latitude orbits passing through the
102 night-side region under near-equinoctial conditions (when the warping of the night-side
103 current sheet is not strong [e.g., Arridge et al., 2008]). For context, the plasma ion and
104 electron data from the Cassini plasma spectrometer (CAPS) [Young et al., 2004] are also
105 presented for one of the intervals examined.
106 Figure 1 shows plasma and magnetic field measurements from CAPS and MAG
107 for a three-day interval in 2010 when Cassini was inbound at near-zero latitude and a
108 local time of ~21 hours. During these three days the spacecraft moved from 31.5 to 12.8
109 $R_s$ in radial distance from Saturn (1 $R_s$ = 60268 km). Panels a) and b) show intermittent
110 enhancements in the plasma fluxes, many associated with recurring encounters with the
111 equatorially confined plasma sheet. Panels c)-f) of the figure show the magnetic field
112 components in the KRTP coordinate system ($B_r$, $B_\theta$, $B_\phi$), and the bottom panel shows the
113 field magnitude. The KRTP system is a spherical polar coordinate system referenced to
114 Saturn's spin axis and is very useful for studying the tail current sheet [e.g., Jackman et
115 al., 2009]. In particular, the radial component provides a clear indication of whether the

116 spacecraft is located north of the tail current sheet ($B_r$ >0) or south of it ($B_r$ <0). The
117 times where Br passes through zero are the times when the spacecraft is crossing the
118 current sheet and are generally associated with enhancements in the plasma flux [e.g.,
119 Szego et al., 2012].
120 Figure 1c shows that during this three-day interval, the current sheet repeatedly
121 swept up and down across Cassini, with a clear periodicity of ~10.7 h (double-headed
122 arrow in the upper portion of that panel), with the radial component of the field
123 periodically changing from positive to negative and back to positive again. That
124 periodicity is reflected as well in the other components and in the field magnitude. These
125 periodic encounters with the current sheet reflect the oscillatory motion of the tail
126 structure that is one of the clear features of Saturn's puzzling planetary period oscillations
127 discussed above (and modeled in work such as Arridge et al. [2011]). In addition to the
128 large-scale oscillations, there are numerous shorter-scale variations in Br, indicating brief
129 approaches to or penetrations of the current sheet. These do not appear to be systematic,
130 and we assume they reflect more rapid fluctuations in the location of the current sheet,
131 perhaps due to propagating waves. In this work we are primarily interested in the
132 planetary period oscillations.
133 Another feature of the $B_r$ signature of the large-scale current sheet crossings seen
134 in Figure 1 is a clear asymmetry between the north-to-south and south-to-north crossings.
135 When the spacecraft moves from the southern hemisphere ($B_r$ <0) to the northern
136 hemisphere ($B_r$ >0), it does so quite rapidly, whereas the reverse transition appears to be

137 much more gradual. A similar asymmetry is reflected in the $B_\phi$ component, which shows
138 an almost sawtooth-like behavior.
139 Cassini's 2010 season featured eighteen orbits (Revs 124-142) with
140 characteristics very similar to the one that produced the data in Figure 1. Figure 2 shows
141 the radial magnetic field component for 5-day intervals from each of those orbits. In
142 every case the signature of the periodic approach to or crossing of the current sheet is
143 evident, as Br periodically nears or crosses zero. (The interval featured in Figure 1 is
144 indicated by the arrow in the right-hand margin of Figure 2a.) Figure 2 shows a wide
145 diversity of $B_r$ signatures: Some show an asymmetry similar to that seen in Figure 1 (e.g.,
146 doy 151-152, doy 167-168). Others show the opposite asymmetry, i.e., slow south-to-
147 north and more rapid north-to-south transitions (e.g., doy 40-43, doy 95-96). Still others
148 seem to be roughly symmetric (e.g., doy 56-59, doy115-117). And yet others are
149 indeterminate, or the spacecraft only approaches but doesn't actually cross the current
150 sheet.
151
152 Discussion
153 Asymmetric crossings of the current sheet, in which the passage in one direction
154 is faster than the return passage, would not be expected from a simple periodic flapping
155 up and down of an otherwise rather uniform current sheet. Two possible scenarios that
156 could produce such an asymmetry are illustrated schematically in Figure 3. Both cases
157 are meant to illustrate how the z-extent of the current sheet varies at a particular local
158 time as the current sheet rotates at a uniform rate around the planet. The phase is thus
159 related to the time, with 360˚ corresponding to a full rotational period. Figure 3a shows

160 the case where a current sheet has a sinusoidally varying vertical (z) displacement but
161 also varies periodically in thickness, such that it is thickest at zero phase and thinnest at a
162 phase of 180 degrees. Figure 3b illustrates the radial field component that would be
163 observed at z=0 as the structure in Figure 3a is swept past an observing spacecraft. The
164 field model is a very simple one with constant (but opposite) values of $B_r$ in the lobes
165 outside of the current-sheet boundaries marked by the red curves in Figure 3a, and with a
166 linear variation from one lobe to the other across the current sheet between the red
167 curves, with $B_r$ =0 at the blue curve. The results in Figure 3b illustrate what one would
168 qualitatively expect: The transition from the south lobe to the north lobe at a phase of 180
169 degrees (thin current sheet) is considerably sharper than the transition from north to south
170 lobes near zero phase (thick current sheet). Figures 3c and 3d illustrate that a similar
171 asymmetry in the south-to-north and north-to-south crossings could arise if the current
172 sheet itself is particularly steep in some phase range, even if the current sheet is
173 uniformly thick.

174 The two scenarios presented in Figure 3 are just illustrative of a range of possible
175 conditions that might give rise to asymmetric current sheet crossings. Other possibilities
176 include propagating pressure waves that cause current-sheet stretching and vertical
177 motions [e.g., Kivelson and Jia, 2014; Jia and Kivelson, 2012]. From single-point
178 measurements it would be difficult to distinguish between any of these scenarios, but
179 analytical and numerical models offer insight into what may be the actual physical cause
180 of the asymmetric crossings. As mentioned in the introduction, both the DRC and the
181 AV models predict not only periodic vertical motion of the current sheet (accounting for
182 the periodic crossings seen in Figures 1 and 2), but periodic variations in the thickness of

183 the current sheet as well. The current sheet thickness in the AV model is measured by the
184 scale height of a fit of the simulated field to a Harris sheet function [Jia and Kivelson,
185 2012] and in the DRC model can be specified [Cowley et al., 2016b] as the sum of three
186 terms: a uniform thickness of the underlying current sheet, plus contributions from both
187 the southern rotating dipole and the northern rotating dipole. As described fully in
188 Cowley et al. [2016b], for the illustrative examples in that paper the undisturbed current
189 sheet half-thickness (2.5 Rs) and oscillation amplitude ( 4 Rs for the southern system)
190 were chosen based on fits done to tail observations by Arridge et al. [2011]. In both
191 models, the northern and southern sources rotate at different rates and hence at times add
192 together and at other times counteract each other in their effects on the current sheet
193 thickness. The resulting effects on the location and thickness of the current sheet can be
194 seen in Figure 9b of Jia and Kivelson [2012] and in Figures 3-6 of Cowley et al. [2016b].
195 In both models both the z position and the thickness of the current sheet vary with the
196 planetary period, with an amplitude that depends on the relative phase between the north
197 and south current sources and is modulated at the beat frequency between them.
198 Because of the time-varying position and thickness of the current sheet, both the
199 DRC and AV models result in a complicated temporal variability in the magnetic field at
200 any given location in the magnetosphere, and the magnetic signature depends on the
201 relative phase of the north and south current sources. The left-hand column of Figure 4
202 illustrates how the radial magnetic field component varies with southern phase (as a
203 proxy for time) within the analytical model of Cowley et al. [2016b], which is designed
204 to represent the behavior of the two current sources in the DRC model. In each panel, the
205 radial component of the field is shown as a function of phase at three different positions

206 relative to the nominal z=0 plane (z=0 and z=±2.5 $R_s$). The different panels correspond
207 to different values of the relative phase ($\Phi_N$-$\Phi_S$, listed along the left-hand margin), where
208 the north and south phases are defined as described in Cowley et al. [2016b]: Both phases
209 increase linearly with time as viewed by a stationary observer (hence in a left-hand sense
210 with respect to Saturn's spin axis), and the zero phase value of each system occurs where
211 its equatorial perturbation field is radially outward.

212 The right-hand column of Figure 4 shows the radial magnetic field component
213 measured at the location r=20 $R_s$ and LT=21 (chosen for direct comparison with the
214 Cassini data in Figure 1) in the global MHD simulation of Jia and Kivelson [2012]. The
215 different panels correspond to times within the simulation when the relative phases of the
216 northern and southern vortices were approximately as given in the left-hand margin of the
217 figure. Note that the phases of the two systems were defined by Jia and Kivelson [2012]
218 to increase in a right-hand sense relative to Saturn's north pole, i.e., the negative of the
219 phases defined by Cowley et al. [2016b] and previous discussions of the DRC model
220 [c.f., Equation 2 of Jia and Kivelson, 2012]. Thus, we have selected the panels in Figure
221 4 (RHS) from times where the phase differences defined within the code are the negative
222 of the values shown in the left-hand margin of Figure 4 (modulo 360).

223 There are strong qualitative similarities between the two columns in Figure 4:
224 Both models exhibit periodic northward and southward crossings of the current sheet, as
225 indicated by the recurrent reversals of the $B_r$ component; and the $B_r$ signatures in both
226 models show considerable diversity, with the character varying with the relative phase.
227 Both the amplitude of the $B_r$ variations and the symmetry (or asymmetry) of the
228 northward vs. southward crossings vary systematically with $\Phi_N$-$\Phi_S$. For relative phases

229 of 165˚ and 195˚, both the DRC and AV models show low-amplitude variations in $B_r$. At
230 relative phases of 90˚ and 135˚, both models show larger-amplitude variations, with a
231 distinct asymmetry between the south-to-north crossings (rapid) and the north-to-south
232 crossings (slow). The opposite asymmetry occurs for 225˚ and to a lesser extent 270˚. At
233 315˚ the crossings are more symmetric. Thus, both models appear able to reproduce
234 qualitatively the variety of $B_r$ signatures seen in the Cassini observations of Figure 2, and
235 the organizing property is the relative phase between the north and south current sources.
236 To test whether the relative phase of the north and south current sources might
237 likewise organize the character of the magnetic field signatures seen in the Cassini data
238 (Figure 2), we use the time-dependent north and south system phases derived from the
239 Cassini magnetic field data by Provan et al. [2011] and Andrews et al. [2012] (see, e.g.,
240 Jackman et al. [2016] for discussion of the link between northern and southern phases
241 and the occurrence of tail reconnection events). The phase angle is the azimuth about
242 Saturn's spin axis, relative to noon, at which the equatorial perturbation field from each
243 current source points radially outward from Saturn. Jackman et al. [2016] adopted an
244 additional correction to the phases to account for the radial propagation of the
245 perturbation field signal, but since our interest is in the relative phase difference between
246 the two systems, that correction would cancel out and can be ignored. Likewise, the
247 dependence of the individual phases on local time also cancels out when the relative
248 phase is computed. Each of the intervals in Figure 2 is assigned a value of the relative
249 phase $\Phi_N$-$\Phi_S$ appropriate to the center time of the interval, as listed in Table 1.
250 Further, each interval is assigned a "character" based on visual inspection of the
251 Br signature. We use four values of the character: Indet=Indeterminate, FN/SS=Fast

South-to-North Crossing/Slow North-to-South Crossing, Symm=Symmetric, SN/FS=Slow South-to-North Crossing/Fast North-to-South Crossing, where the direction refers to the apparent motion of the spacecraft (e.g., negative $B_r$ followed by positive $B_r$ corresponds to a south-to-north crossing). Because the determination of the character of the crossings is subjective, we compile the assessments of two independent observers. The resulting characters are listed in Table 1 for the full set of intervals shown in Figure 2.

Figure 5 is a graphical summary of the phase differences and characters listed in Table 1. Also shown in Figure 5 are similar assessments of the $B_r$ signatures shown for the two models in Figure 4, performed by the same two independent observers whose character identifications are listed in Table 1. With the exception of just a few points, it is clear from Figure 5 that the relative phase of the two current systems does indeed order the character of the Br signatures seen by Cassini, in the same sense that emerges for both the DRC and AV models: Asymmetric current sheet crossings in which the northbound crossing occurs more rapidly than the southbound crossing (character=FN/SS) are seen when the relative phase lies between 0˚ and 180˚, while the reverse asymmetry is seen between 180˚ and 360˚. Symmetric crossings, with a couple of exceptions, occur near 0˚ and 180˚.

It should be noted that asymmetric structure in the $B_r$ profiles for northward vs. southward crossing of the current sheet is also found in the AV model even when it is run with only a single atmospheric vortex [Jia et al., 2012], as illustrated in Figure 6. The variation of $B_r$ from an AV run with a source only in the south arises from the combination of a periodically varying current sheet thickness and a periodically varying

275 current sheet position, which are dynamical changes arising from compressional waves
276 generated by the vortical ionospheric flow and propagating through the magnetotail
277 [Kivelson and Jia, 2014]. Importantly, these variations, while periodic, are not sinusoidal
278 and are not in phase with each other as assumed by the DRC formalism (Figure 6a). The
279 primary asymmetry arises because the current sheet moves southward from z = 0 to z = -
280 0.5 $R_S$ much more rapidly than it returns northward from -0.5 $R_S$ to 0 $R_S$, a behavior
281 similar to that depicted in Figure 3c. The current sheet is thicker when it approaches z=0
282 going southward than when it approaches z=0 going northward, but this produces only a
283 small bump in the $B_r$ profile. Thus, it is not necessary to have current sources in both
284 hemispheres to produce asymmetric current sheet crossings per se, but the crucial finding
285 in this study is that the character of the asymmetry varies with time in such a way that it
286 is well organized by the relative phase of a northern and southern source, as inferred from
287 magnetic field measurements, and that variation requires dual sources of changing
288 relative phase. That element of the asymmetry is well captured by both the DRC and the
289 AV model with dual sources (Jia and Kivelson, 2012). We believe that the nonsinusoidal
290 variation of the thickness and position of the current sheet is probably responsible for the
291 double-humped substructure that appears in a number of the Br profiles from the AV
292 model in Figure 4.
293 The clear dependence in Figure 5 of the character of the current sheet crossings on
294 the relative phase of the two perturbation current systems provides additional
295 observational support to the DRC and AV models of the planetary period oscillations.
296 The observed asymmetries in the crossings are thus quite consistent with periodic
297 variations of both the location and thickness of the tail current sheet as predicted by both

298 models and previously inferred from other data [e.g., Morooka et al., 2009; Provan et al.,
299 2012].

300 The discussion above emphasized the importance of the relative phase of the two
301 current systems in determining the nature of the current sheet crossing. However, as
302 described in detail by Cowley et al. [2016b], another similarly important parameter is the
303 relative amplitudes of the two current systems. As shown in that study, asymmetric
304 ("sawtooth"-like) crossings are most pronounced for near-equal amplitudes of the two
305 systems. For the DRC calculations shown in the left-hand column of Figure 4, a north-
306 to-south amplitude ratio of 1:1 was used, producing a very marked asymmetry. In the
307 AV simulation that produced the right-hand column, the ratio of northern vortex current
308 density to southern was only 1:3 [Jia and Kivelson, 2012], and we might expect a smaller
309 asymmetry, but at least in the range of $\Phi_N$-$\Phi_S$~0-180˚ the asymmetry is quite evident.

310 With regard to the observations, fits to Cassini magnetometer data have found that
311 the ratio of the north and south current densities varies substantially on the time scale of
312 months [Andrews et al., 2012; Provan et al., 2013; Cowley et al., 2016b]. During the
313 2010 season shown in Figure 2 the ratio of the north to south perturbation field
314 amplitudes was found to be ~1.03, consistent with the clear asymmetries seen when the
315 relative phases were favorable (Figure 5). However, as discussed by Cowley et al.
316 [2016b], there were other intervals in the Cassini mission during which the ratio was
317 significantly different from 1.0, which might be suitable for examining this dependence.
318 In particular, low-latitude, night-side passes somewhat similar to those in 2010 occurred
319 in 2006, 2009, and 2015 [c.f., Figure 1 of Cowley et al., 2016b], and we have examined

320 MAG data from these periods as well. Unfortunately, for a combination of reasons we
321 note below, the observations from those intervals were less than ideal for this study.
322 During 2006 the derived ratio of field amplitudes was 0.38 [Andrews et al., 2012],
323 for which less asymmetry in N->S vs S->N crossings might be expected [Cowley et al.,
324 2016b]. An examination of the intervals of multiple current sheet crossings from the
325 2006 Cassini tail season similar to Figure 2 reveals no evidence for clear and repeated
326 asymmetric crossings. In part this is because the spacecraft orbit and current sheet
327 deflection [e.g., Arridge et al., 2008] were such that many of the current sheet encounters
328 were just brief dips into the field reversal region, rather than full-blown crossings back
329 and forth. At other times the orbit was such that there was only a single transition from
330 the northern hemisphere to the southern, without the multiple back-and-forth crossings
331 needed to establish the character of the northward vs. southward crossings. Still other
332 intervals showed rather disturbed fields, with no clear pattern of crossings or character.
333 Nonetheless, during the few intervals when the crossings were suitable to determine the
334 character, no pronounced asymmetries were observed.
335 We have also examined the Br data for current sheet crossings in 2009, when the
336 inferred N/S amplitude ratio was 0.87 for the first half of the year and 1.02 for the second
337 half [Andrews et al., 2012], both apparently favorable for pronounced asymmetries.
338 While many of the crossings were again single transitions from one hemisphere to the
339 other, particularly in the first half of the year, there were several intervals with repeated
340 crossings. Two of those showed FN/SS asymmetries like those in Figure 2, but generally
341 weaker. The relative phase of the N and S systems for those intervals was 48˚ and 65˚,
342 consistent with the relationship shown in Figure 5. There were three sets of crossings that

were more nearly symmetric, and they had relative phases of 279˚, 287˚ and 304˚, consistent with other symmetric crossings found in 2010 (Figure 5). None of the 2009 intervals that were suitable for examining the symmetry of the crossings were of the SN/FS character.

Finally, we examined the Br data for 2015, when the inferred N/S amplitude was >2 [Provan et al., 2016; see also Cowley et al., 2016], for which little asymmetry would be expected. Again there were very few intervals of repeated crossings that would be suitable to determine the character of the crossings. Only three sets of repeated crossings were found to be useful, and all three intervals (corresponding to relative phases of 45˚, 130˚, and 330˚) were essentially symmetric with respect to northward and southward crossings. Examination of Figure 5 suggests that, while crossings at 45˚ and 330˚ might well be expected to be symmetric, the event at 130˚ should have been FN/SS if it followed the 2010 trend. Thus, this one event seems to support the expectation that N/S amplitude ratios well away from 1.0 would not produce a pronounced asymmetry.

While the observing conditions were not ideal during 2006, 2009, and 2015, the observation of clear asymmetries in 2010 and a few asymmetries in 2009, while none was seen in 2006 or 2015, is at least modestly consistent with the expectation of stronger asymmetries for nearly equal amplitudes of the N and S systems, as discussed by Cowley et al. [2016b].

## Summary

Repeated crossings of Saturn's magnetospheric current sheet observed by the Cassini spacecraft during 2010 often display asymmetries such that the northbound

366 crossing occurs faster than the southbound crossing or vice versa, while at other times the
367 crossings are more symmetric. The character of the crossings is well organized by the
368 relative phase of the northern vs. southern perturbation currents inferred in earlier
369 analyses of the magnetic field observations [e.g., Andrews et al., 2012; Provan et al.,
370 2012]. Further, the dependence of the character on the relative phase is consistent with
371 similar asymmetries predicted by the dual rotating current systems inferred from those
372 magnetic field observations [Cowley et al., 2016b] and predicted by global MHD models
373 that incorporate the effects of hypothesized atmospheric vortices [e.g., Jia and Kivelson,
374 2012]. We thus conclude that the observed asymmetries are consistent with a periodic
375 thickening and thinning of the magnetospheric current sheet as predicted by these two
376 models.

377 Current sheet crossings observed in 2006, 2009, and 2015 are also basically
378 supportive of theoretical expectations [Cowley et al., 2016b] that asymmetric crossings
379 should be most pronounced during epochs when the perturbation amplitudes of the two
380 current systems are near-equal. However, because of the nature and orientation of the
381 orbits during these years, Cassini spent less time near the current sheet, and the effect is
382 less definitively visible. It is further likely that other effects (e.g., solar wind pressure
383 variations) may also affect the location and apparent thickness of the current sheet,
384 yielding a few discrepancies between the observations and expectations. Nonetheless,
385 the evidence presented here is clearly consistent with the periodic thickening and thinning
386 of Saturn's magnetospheric current sheet in response to perturbations produced by the
387 current systems hypothesized in earlier studies.
388

Acknowledgements

This work emerged from collaborative discussions that took place during a visit of MFT to the University of Southampton as a Diamond Jubilee Fellow. The support provided by the Diamond Jubilee Fellowship is gratefully acknowledged. Work at PSI was supported by the NASA Cassini program through JPL contract 1243218 with Southwest Research Institute. The Cassini project is managed by the Jet Propulsion Laboratory for NASA. CMJ is supported by a Science and Technology Facilities Council Ernest Rutherford Fellowship ST/L004399/1. Work at the University of Leicester was supported by STFC Consolidated Grant ST/N000749/1. MGK is supported by NASA grant NNX14AG87G:000002. Work by XJ is supported by NASA grant NNX12AK34G. All Cassini magnetometer and plasma data used for this study are available from the Planetary Data System (http://pds.nasa.gov/).

References

Andrews, D. J., E. J. Bunce, S. W. H. Cowley, M. K. Dougherty, G. Provan, and D. J. Southwood (2008), Planetary period oscillations in Saturn's magnetosphere: Phase relation of equatorial magnetic field oscillations and Saturn kilometric radiation modulation, *J. Geophys. Res., 113,* A09205, doi:10.1029/2007JA012937.

Andrews, D. J., A. J. Coates, S. W. H. Cowley, M. K. Dougherty, L. Lamy, G. Provan, and P. Zarka (2010), Magnetospheric period oscillations at Saturn: Comparison of equatorial and high latitude magnetic field periods with north and south Saturn

412 kilometric radiation periods, *J. Geophys. Res., 115,* A12252,
413 doi:10.1029/2010JA015666.
414 Andrews, D. J., S. W. H. Cowley, M. K. Dougherty, L. Lamy, G. Provan, and D. J.
415 Southwood (2012), Planetary period oscillations in Saturn's magnetosphere:
416 Evolution of magnetic oscillation properties from southern summer to post-
417 equinox, *J. Geophys. Res., 117*, A04224, doi:10.1029/2011JA017444.
418 Arridge, C. S., K. K. Khurana, C. T. Russell, D. J. Southwood, N. Achilleos, M. K.
419 Dougherty, A. J. Coates, and H. K. Leinweber (2008), Warping of Saturn's
420 magnetospheric and magnetotail current sheets, *J. Geophys. Res., 113,* A08217,
421 doi:10.1029/2007JA012963.
422 Arridge, C. S., et al. (2011), Periodic motion of Saturn's nightside plasma sheet, *J.*
423 *Geophys. Res., 116,* A11205, doi:10.1029/2011JA016827.
424 Brandt, P. C., K. K. Khurana, D. G. Mitchell, N. Sergis, K. Dialynas, J. F.Carbary, E. C.
425 Roelof, C. P. Paranicas, S. M. Krimigis, and B. H. Mauk (2010), Saturn's periodic
426 magnetic field perturbations caused by a rotating partial ring current, *Geophys.*
427 *Res. Lett., 37*, L22103, doi:10.1029/ 2010GL045285.
428 Burch, J. L., A. D. DeJong, J. Goldstein, and D. T. Young (2009), Periodicity in Saturn's
429 magnetosphere: Plasma cam, *Geophys. Res. Lett., 36,* L14203,
430 doi:10.1029/2009GL039043.
431 Carbary, J. F., and S. M. Krimigis (1982), Charged particle periodicity in the Saturnian
432 magnetosphere, *Geophys. Res. Lett., 9*(9), 1073–1076,
433 doi:10.1029/GL009i009p01073.
434 Carbary, J. F., and D. G. Mitchell (2013), Periodicities in Saturn's magnetosphere, *Rev.*

435 *Geophys.,* 51, 1–30, doi:10.1002/rog.20006.
436 Carbary, J. F., D. G. Mitchell, S. M. Krimigis, D. C. Hamilton, and N. Krupp (2007),
437 Charged particle periodicities in Saturn's outer magnetosphere, *J. Geophys. Res.,*
438 *112*, A06246, doi:10.1029/2007JA012351.
439 Carbary, J. F., D. G. Mitchell, P. Brandt, C. Paranicas, and S. M. Krimigis (2008), ENA
440 periodicities at Saturn, *Geophys. Res. Lett., 35,* L07102,
441 doi:10.1029/2008GL033230.
442 Cowley, S. W. H., D. M. Wright, E. J. Bunce, A. C. Carter, M. K. Dougherty, G.
443 Giampieri, J. D. Nichols, and T. R. Robinson (2006), Cassini observations of
444 planetary-period magnetic field oscillations in Saturn's magnetosphere: Doppler
445 shifts and phase motion, *Geophys. Res. Lett., 33,* L07104,
446 doi:10.1029/2005GL025522.
447 Cowley, S. W. H., P. Zarka, G. Provan, L. Lamy, and D. J. Andrews (2016a), Comment
448 on "A new approach to Saturn's periodicities" by J. F. Carbary, *J. Geophys. Res.,*
449 *121,* 2418, doi:10.1002/2015JA021996.
450 Cowley, S. W. H., G. Provan, G. J. Hunt, and C. M. Jackman (2016b), Planetary period
451 modulations of Saturn's magnetotail current sheet: A simple illustrative
452 mathematical model, *J. Geophys. Res.,* in press.
453 Desch, M. D., and M. L. Kaiser (1981), Voyager measurement of the rotation period of
454 Saturn's magnetic field, *Geophys. Res. Lett., 8,* 253–256.
455 Dougherty, M. K., et al. (2004), The Cassini magnetic field investigation, *Space Sci.*
456 *Rev., 114*, 331–383, doi:10.1007/s11214-004-1432-2.
457 Espinosa, S. A., and M. K. Dougherty (2000), Periodic perturbations in Saturn's

458 magnetic field, *Geophys. Res. Lett., 27*, 2785–2788, doi:10.1029/2000GL000048.
459 Espinosa, S. A., D. J. Southwood, and M. K. Dougherty (2003), How can Saturn impose
460 its rotation period in a noncorotating magnetosphere?, *J. Geophys. Res., 108*(A2),
461 1086, doi:10.1029/2001JA005084.
462 Galopeau, P. H. M., and A. Lecacheux (2000), Variations of Saturn's radio rotation
463 period measured at kilometer wavelengths, *J. Geophys. Res., 105,* 13089–13101.
464 Goldreich, P., and A. J. Farmer (2007), Spontaneous axisymmetry breaking of the
465 external magnetic field at Saturn, *J. Geophys. Res., 112*, A05225,
466 doi:10.1029/2006JA012163.
467 Gurnett, D. A., A. M. Persoon, W. S. Kurth, J. B. Groene, T. F. Averkamp, M. K.
468 Dougherty, and D. J. Southwood (2007), The variable rotation period of the inner
469 region of Saturn's plasma disk, *Science, 316*(5823), 442–445,
470 doi:10.1126/science.1138562.
471 Gurnett, D. A., A. Lecacheux, W. S. Kurth, A. M. Persoon, J. B. Groene, L. Lamy, P.
472 Zarka, and J. F. Carbary (2009), Discovery of a north-south asymmetry in
473 Saturn's radio rotation period, *Geophys. Res. Lett., 36,* L16102,
474 doi:10.1029/2009GL039621.
475 Hunt , S. W. H. Cowley, G. Provan, E. J. Bunce, I. I. Alexeev, E. S. Belenkaya, V. V.
476 Kalegaev, M. K. Dougherty, and A. J. Coates (2015), Field-aligned currents in
477 Saturn's southern nightside magnetosphere: Subcorotation and planetary period
478 oscillation components, *J. Geophys. Res., 119*, 9847-9899,
479 doi:10.1002/2014JA020506.
480 Jackman, C. M., C. S. Arridge, H. J. McAndrews, M. G. Henderson, and R. J. Wilson

481 (2009), Northward field excursions in Saturn's magnetotail and their relationship
482 to magnetospheric periodicities, *Geophys. Res. Lett., 36,* L16101, doi:10.1029/
483 2009GL039149.
484 Jackman, C. M., G. Provan, and S. W. H. Cowley (2016), Reconnection events in
485 Saturn's magnetotail: Dependence of plasmoid occurrence on planetary period
486 oscillation phase, *J. Geophys. Res*., *121*, 2922-2934, doi: 10.1002/2015JA021985.
487 Jia, X., and M. G. Kivelson (2012), Driving Saturn's magnetospheric periodicities from
488 the upper atmosphere/ ionosphere: Magnetotail response to dual sources, *J.*
489 *Geophys. Res., 117*, A11219, doi:10.1029/2012JA018183.
490 Jia, X., M. G. Kivelson, and T. I. Gombosi (2012), Driving Saturn's magnetospheric
491 periodicities from the upper atmosphere/ionosphere, *J. Geophys. Res., 117*,
492 A04215, doi:10.1029/2011JA017367.
493 Khurana, K. K., D. G. Mitchell, C. S. Arridge, M. K. Dougherty, C. T. Russell, C.
494 Paranicas, N. Krupp, and A. J. Coates (2009), Sources of rotational signals in
495 Saturn's magnetosphere, *J. Geophys. Res., 114,* A02211,
496 doi:10.1029/2008JA013312.
497 Kivelson, M. G., and X. Z. Jia (2014), Control of periodic variations in Saturn's
498 magnetosphere by compressional waves, *J. Geophys. Res., 119,* 8030, doi:
499 10.1002/2014JA020258.
500 Kurth, W. S., T. F. Averkamp, D. A. Gurnett, J. B. Groene, and A. Lecacheux (2008), An
501 update to a Saturnian longitude system based on kilometric radio emissions, *J.*
502 *Geophys. Res., 113*, A05222, doi:10.1029/2007JA012861.
503 Lamy, L. (2011), Variability of southern and northern SKR periodicities, in Planetary

504 Radio Emissions VII, edited by H. O. Rucker, W. S. Kurth, P. Louarn, and G.
505 Fischer, pp. 39–50, Austrian Acad. Sci. Press, Vienna.
506 Mitchell, D. G., et al. (2009a), Recurrent energization of plasma in the midnight-to-dawn
507 quadrant of Saturn's magnetosphere, and its relationship to auroral UV and radio
508 emissions, *Planet. Space Sci., 57*, 1732–1742, doi:10.1016/j.pss.2009.04.002.
509 Mitchell, D. G., J. F. Carbary, S. W. H. Cowley, T. W. Hill, and P. Zarka (2009b), The
510 dynamics of Saturn's magnetosphere, in *Saturn From Cassini-Huygens*, edited by
511 M. K. Dougherty, L. W. Esposito, and S. M. Krimigis, pp. 257–279, Springer,
512 New York, doi:10.1007/978-1-4020-9217-6_10.
513 Morooka, M. W., et al. (2009), The electron density of Saturn's magnetosphere, *Ann.*
514 *Geophys., 27*, 2971–2991, doi:10.5194/angeo-27-2971-2009.
515 Nemeth, Z., K. Szego, L. Foldy, S.W.H. Cowley, G. Provan, and M. Thomsen (2016),
516 Periodic motion of the magnetodisk as a cause of quasi-periodic variations in the
517 Kronian magnetosphere, *Plan. Space Sci., 130,* 54, doi:10.1016/j.pss.2016.07.002
518 Provan, G., D. J. Andrews, B. Cecconi, S. W. H. Cowley, M. K. Dougherty, L. Lamy,
519 and P. Zarka (2011), Magnetospheric period magnetic field oscillations at Saturn:
520 Equatorial phase 'jitter' produced by superposition of southern- and northern-
521 period oscillations, *J. Geophys. Res., 116,* A04225, doi:10.1029/2010JA016213.
522 Provan, G., D. J. Andrews, C. S. Arridge, A. J. Coates, S. W. H. Cowley, G. Cox, M. K.
523 Dougherty, and C. M. Jackman (2012), Dual periodicities in planetary-period
524 magnetic field oscillations in Saturn's tail, *J. Geophys. Res., 117*, A01209,
525 doi:10.1029/2011JA017104.
526 Provan, G., S. W. H. Cowley, J. Sandhu, D. J. Andrews, and M. K. Dougherty (2013),

527 Planetary period magnetic field oscillations in Saturn's magnetosphere: Post-
528 equinox abrupt non- monotonic transitions to northern system dominance, *J.*
529 *Geophys. Res. Space Physics*, *118*, 3243–3264, doi:10.1002/jgra.50186.
530 Provan, G., S. W. H. Cowley, L. Lamy, E. J. Bunce, G. J. Hunt, P. Zarka, and M. K.
531 Dougherty (2016), Planetary period oscillations in Saturn's magnetosphere:
532 Coalescence and reversal of northern and southern periods in late northern spring,
533 *J. Geophys. Res.,* submitted, doi:10.1002/2016JA023056.
534 Southwood, D. J., and S.W.H. Cowley (2014), The origin of Saturn's magnetic
535 periodicities: Northern and southern current systems, *J. Geophys. Res., 119,* 1563,
536 doi: 10.1002/2013JA019632.
537 Southwood, D. J., and M. G. Kivelson (2007), Saturn magnetospheric dynamics:
538 Elucidation of a camshaft model, *J. Geophys. Res., 112*, A12222,
539 doi:10.1029/2007JA012254.
540 Szego, K., Z. Nemeth, G. Erdos, L. Foldy, Z. Bebesi, M. Thomsen, and D. Delapp
541 (2012), Location of the magnetodisk in the nightside outer magnetosphere of
542 Saturn near equinox based on ion densities, *J. Geophys. Res*., *117*, A09225,
543 doi:10.1029/2012JA017817.
544 Warwick, J. W., D. S. Evans, J. H. Romig, J. K. Alexander, M. D. Desch, M. L. Kaiser,
545 M. Aubier, Y. Leblanc, A. Lecacheux, and B. M. Pedersen (1982), Planetary radio
546 astronomy observations from Voyager-2 near Saturn, *Science, 215,* 582–587.
547 Young, D. T., et al. (2004), Cassini Plasma Spectrometer investigation, *Space Sci. Rev.,*
548 *114*, 1–112.
549

**Table 1.** Character of 2010 Current Sheet Crossings

| DOY Range | R[a] ($R_s$) | Latitude[a] (deg) | Local Time[a] (h) | $\Phi_N$-$\Phi_S$[a] (deg) | Character[b] (Observer 1) | Character[b] (Observer 2) |
|---|---|---|---|---|---|---|
| 4-9 | 33.0 | -14.5 | 19.7 | 115 | Indet | Symm |
| 20-25 | 33.6 | -3.3 | 19.6 | 202 | Indet | Indet |
| 38-43 | 32.7 | 0.1 | 20.1 | 298 | SN/FS | SN/FS |
| 54-59 | 37.1 | 0.1 | 19.7 | 9 | Symm | Symm |
| 75-80 | 24.2 | 0.4 | 20.8 | 94 | FN/SS | FN/SS |
| 92-97 | 27.7 | 0.3 | 20.4 | 168 | SN/FS | SN/FS |
| 112-117 | 29.8 | 0.2 | 20.2 | 269 | Symm | Symm |
| 133-138 | 27.0 | 0.3 | 20.4 | 9 | FN/SS | FN/SS |
| 148-153 | 30.6 | 8.7 | 19.1 | 65 | FN/SS | FN/SS |
| 164-169 | 30.7 | -1.0 | 19.1 | 123 | FN/SS | Indet |
| 180-185 | 30.0 | -13.9 | 19.2 | 168 | Indet | Indet |
| 200-205 | 30.8 | -3.8 | 19.9 | 206 | Symm | Indet |
| 220-225 | 30.4 | -3.8 | 19.9 | 245 | SN/FS | SN/FS |
| 240-245 | 30.5 | -3.9 | 19.9 | 299 | Indet | Indet |
| 260-265 | 30.2 | -3.9 | 19.9 | 339 | Indet | SN/FS |
| 284-289 | 29.3 | -2.8 | 20.6 | 15 | Indet | Indet |
| 328-333 | 32.1 | -0.1 | 19.7 | 104 | FN/SS | FN/SS |
| 349-354 | 30.0 | -0.1 | 19.8 | 118 | Indet | Indet |

[a]Specified at center of interval

[b]Character definitions: Indet=Indeterminate, FN/SS=Fast South-to-North Crossing/Slow

553 North-to-South Crossing, Symm=Symmetric, SN/FS=Slow South-to-North Crossing/Fast

554 North-to-South Crossing

555

556

557 Figure Captions

558 1. Cassini plasma and magnetic field measurements from a three-day interval in 2010,
559 during which the spacecraft made repeated periodic crossings of the tail current sheet. a-
560 b) Color-coded logarithm of the ion and electron count rates (proportional to energy flux)
561 as a function of energy. c-e) Magnetic field r, θ, and ϕ components in the KRTP
562 coordinate system. f) Magnetic field magnitude. Reversals in the r-component of the
563 field indicate crossings of the current sheet from one hemisphere to the other (positive $B_r$
564 indicates northern hemisphere). The double-headed arrow in panel c shows the duration
565 of the ~10.7-h planetary rotation period.

566 2. Radial component of the magnetic field observed by Cassini on 5-day segments of the
567 eighteen orbits of 2010 that featured periodic crossings of the tail current sheet, as
568 indicated by reversals of the sign of $B_r$: a) prior to DOY 153, b) after DOY 164. The
569 arrow in the right-hand column of a) indicates the interval featured in Figure 1.

570 3. Schematic illustration of how asymmetric $B_r$ signatures of northward vs southward
571 crossings of the current sheet could arise from a variable current sheet thickness (a,b) or a
572 steepening of the current sheet in the azimuthal direction (c,d). Panels a and c show the
573 hypothesized vertical location of the center (blue curve) and north and south edges (red
574 curves) of the current sheet as a function of azimuthal phase angle. Panels b and d show
575 the resulting $B_r$ signature that would be observed at a point in the equatorial plane as the
576 corresponding current sheet structure rotated past it. The field structure is taken to be a
577 simple form: constant but opposite values of $B_r$ in the lobes outside of the current sheet

boundaries, with a linear variation from one boundary to the other across the current sheet.

4. Variation of the radial magnetic field component with time for (left column) the DRC model of Cowley et al. [2016b] and (right column) the AV model of Jia and Kivelson [2012]. The different panels show the $B_r$ variation for the different values of the relative phase between the northern and southern current systems ($\Phi_N$-$\Phi_S$) listed along the left-hand margin. The three curves in the DRC panels show the $B_r$ value expected at three different vertical locations relative to the nominal center of the current sheet: Green (z=+2.5 $R_s$), black (z=0), and purple (z=-2.5 $R_s$). The AV panels on the right-hand side are extracted from the position (r=20 $R_s$ and 21 LT) at epochs in the global MHD simulation of Jia and Kivelson [2012] when the relative phase of the two atmospheric vortices is approximately the negative of the values in the left-hand column of the figure (modulo 360) to account for the different handedness of the definition of phase in Jia and Kivelson compared to that used here (which follows Cowley et al. [2016b] and previous related works). The DRC calculations in the left-hand column assume a ratio of north-to-south current densities of 1:1, while the AV simulation in the right-hand column assumed a current density ratio of 1:3.

5. Graphical summary of the character of the current sheet crossings at various values of the relative phase of the north and south current systems as inferred from the 2010 Cassini observations in Figure 2 (black filled and open circles), the AV model of Jia and Kivelson [2012] (red open triangles), and the DRC model of Cowley et al. [2016b] (blue inverted triangles). Character abbreviations correspond to the following: Indet=indeterminate, FN/SS=Fast northward crossing/Slow southward crossing,

601 Symm=Symmetric, SN/FS=Slow northward crossing/Fast southward crossing, where the
602 direction refers to the apparent motion of the spacecraft (e.g., negative $B_r$ followed by
603 positive $B_r$ corresponds to a northward crossing). There are two Cassini points (Cassini 1
604 and Cassini 2, connected by vertical lines) for each of the intervals in Figure 2 and Table
605 1, corresponding to assessments of Figure 2 by two independent observers. This
606 procedure provides a rough guide to the uncertainty of the various determinations.
607 Likewise, the error bars on the AV and DRC points indicate disparities in the
608 determinations by the same two observers.
609 6. From the AV simulation of Jia et al. [2012] at the location (20 Rs, 21 LT): (a) the
610 height in $R_S$ (blue) and the thickness in $R_S$ (green) of the current sheet. (Thickness is
611 evaluated from a fit to a Harris equilibrium model.) (b) The radial component of the
612 magnetic field (Br) at the equator (z=0). Both are plotted vs simulation time in hours.
613

**Figure 1.**

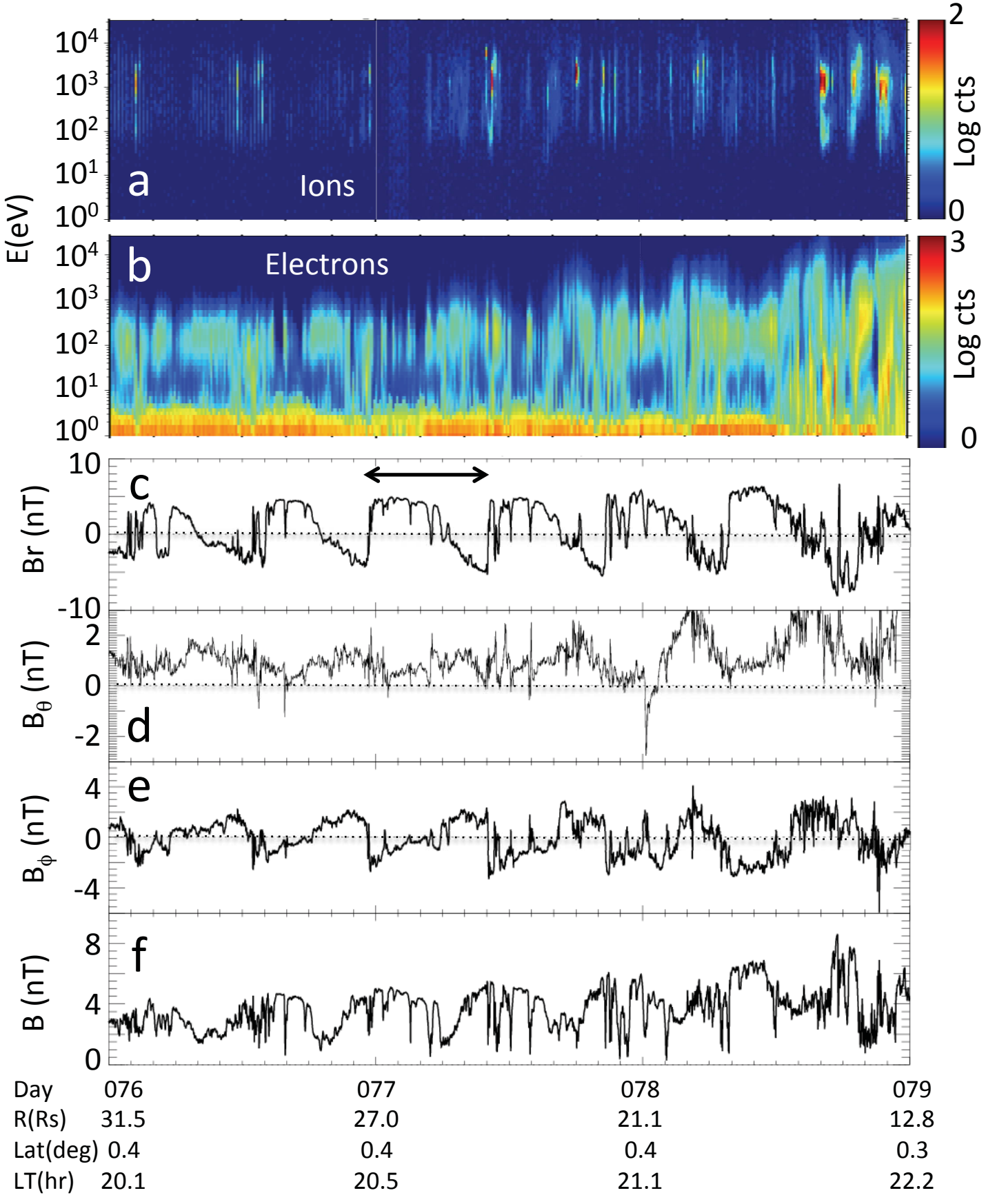
E(eV)
$10^4$
$10^3$
$10^2$
$10^1$
$10^0$
a
Ions
2
Log cts
0
b
Electrons
3
Log cts
0
Br (nT)
10
0
-10
c
$B_\theta$ (nT)
2
0
-2
d
$B_\phi$ (nT)
4
0
-4
e
B (nT)
8
4
0
f
Day 076 077 078 079
R(Rs) 31.5 27.0 21.1 12.8
Lat(deg) 0.4 0.4 0.4 0.3
LT(hr) 20.1 20.5 21.1 22.2

**figure 2.**

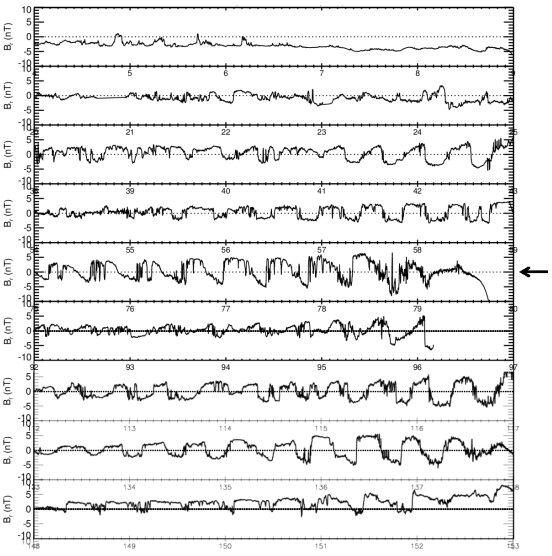


a. DOY 2010

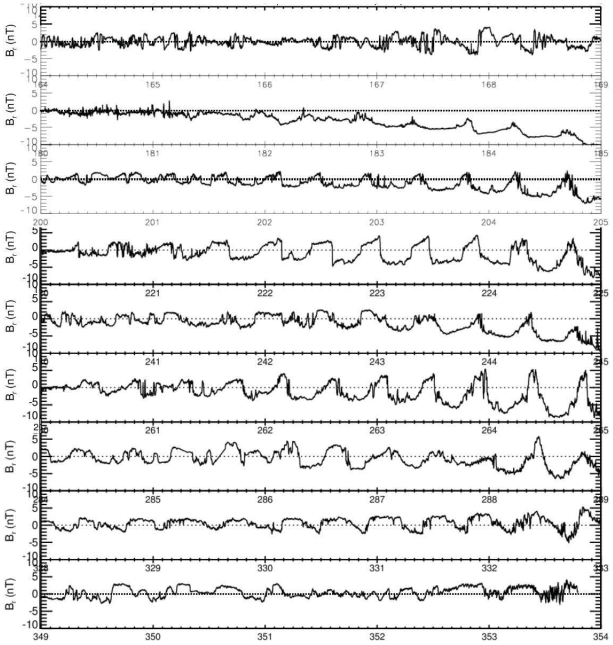


b. DOY 2010

**Figure 3.**

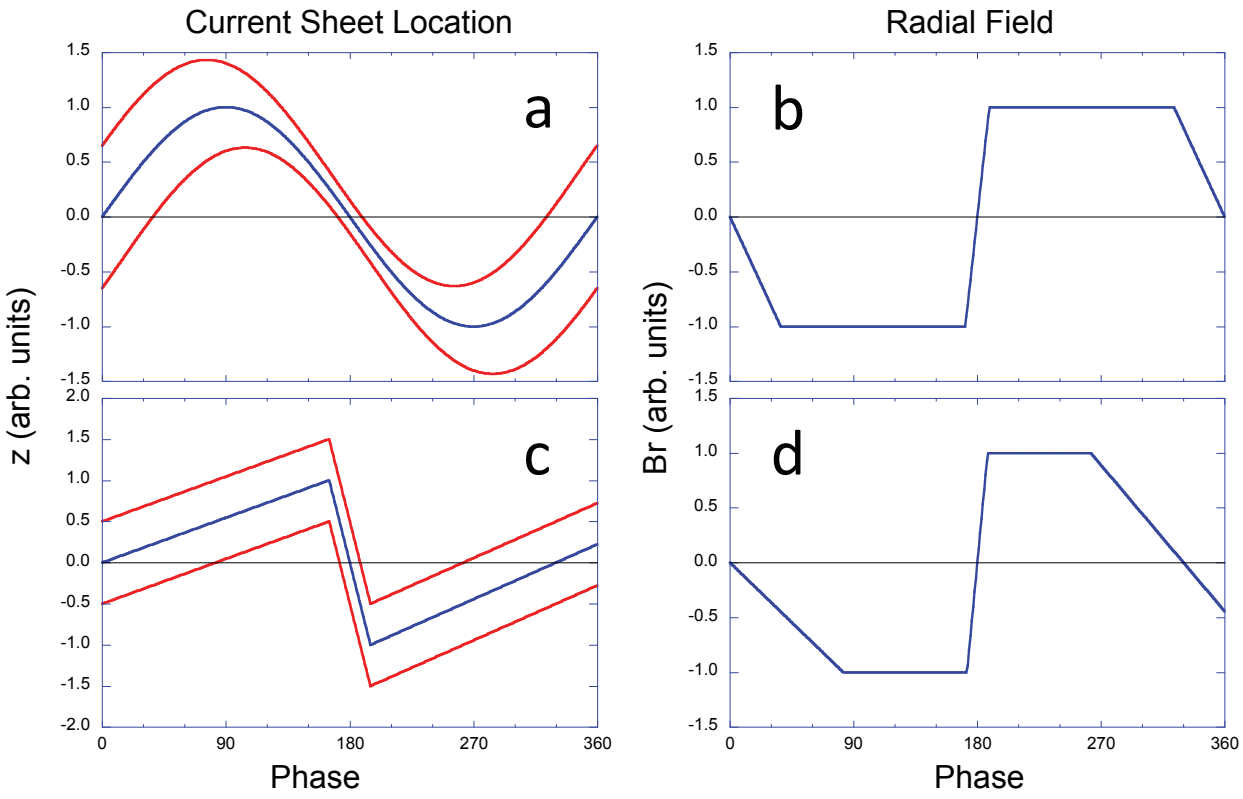
Current Sheet Location
Radial Field
a
b
c
d
z (arb. units)
Br (arb. units)
Phase
Phase
1.5
1.0
0.5
0.0
-0.5
-1.0
-1.5
2.0
-2.0
0
90
180
270
360

**Figure 4.**

| $\Phi_N$-$\Phi_S$ | DRC | AV |
|---|---|---|
| | *Br/Bo* | (r=20, LT=21) |
| a. 45° | 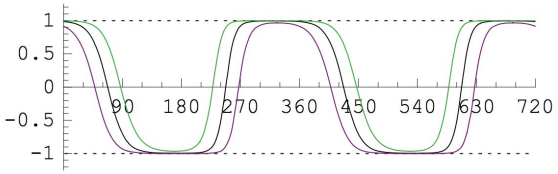 | 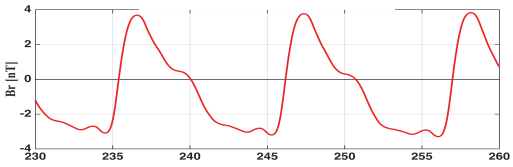 |
| b. 90° | 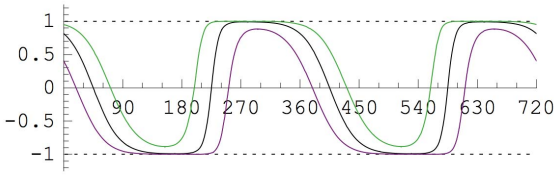 | 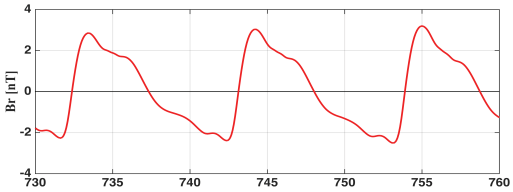 |
| c. 135° | 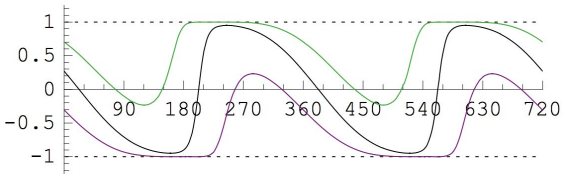 | 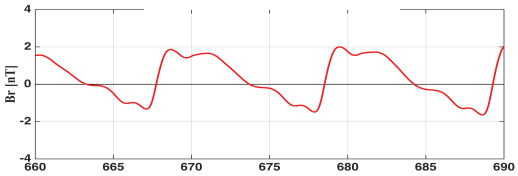 |
| d. 165° | 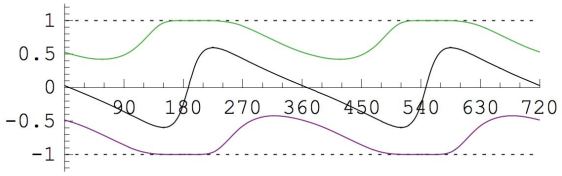 | 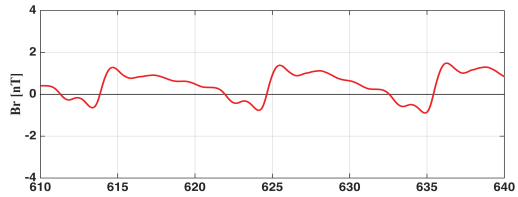 |
| e. 195° | 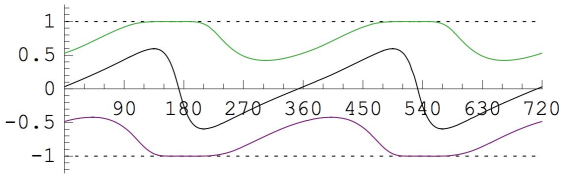 | 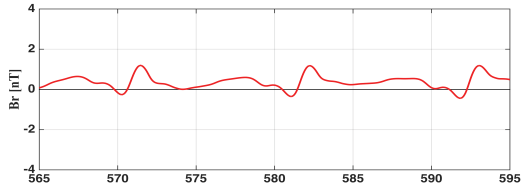 |
| f. 225° | 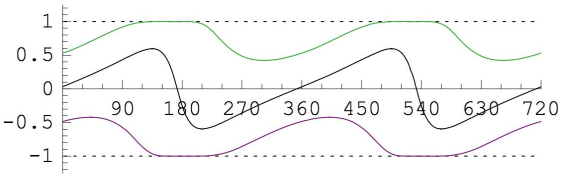 | 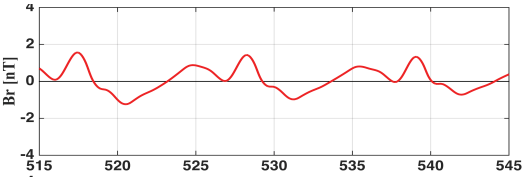 |
| g. 270° | 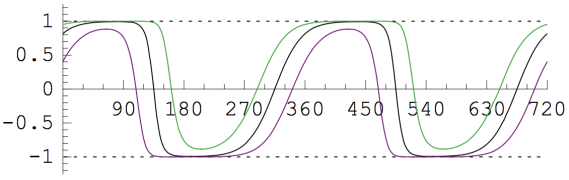 | 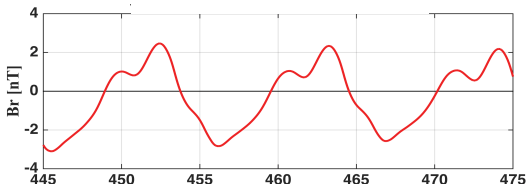 |
| h. 315° | 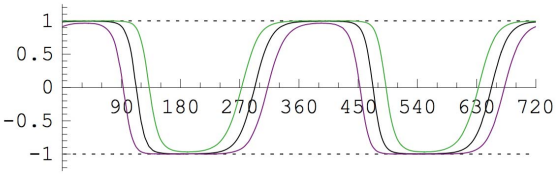 | 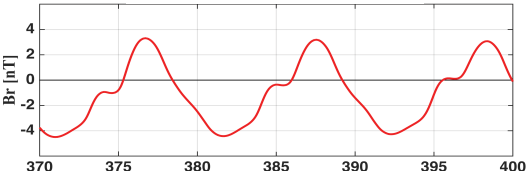 |

**Figure 5.**

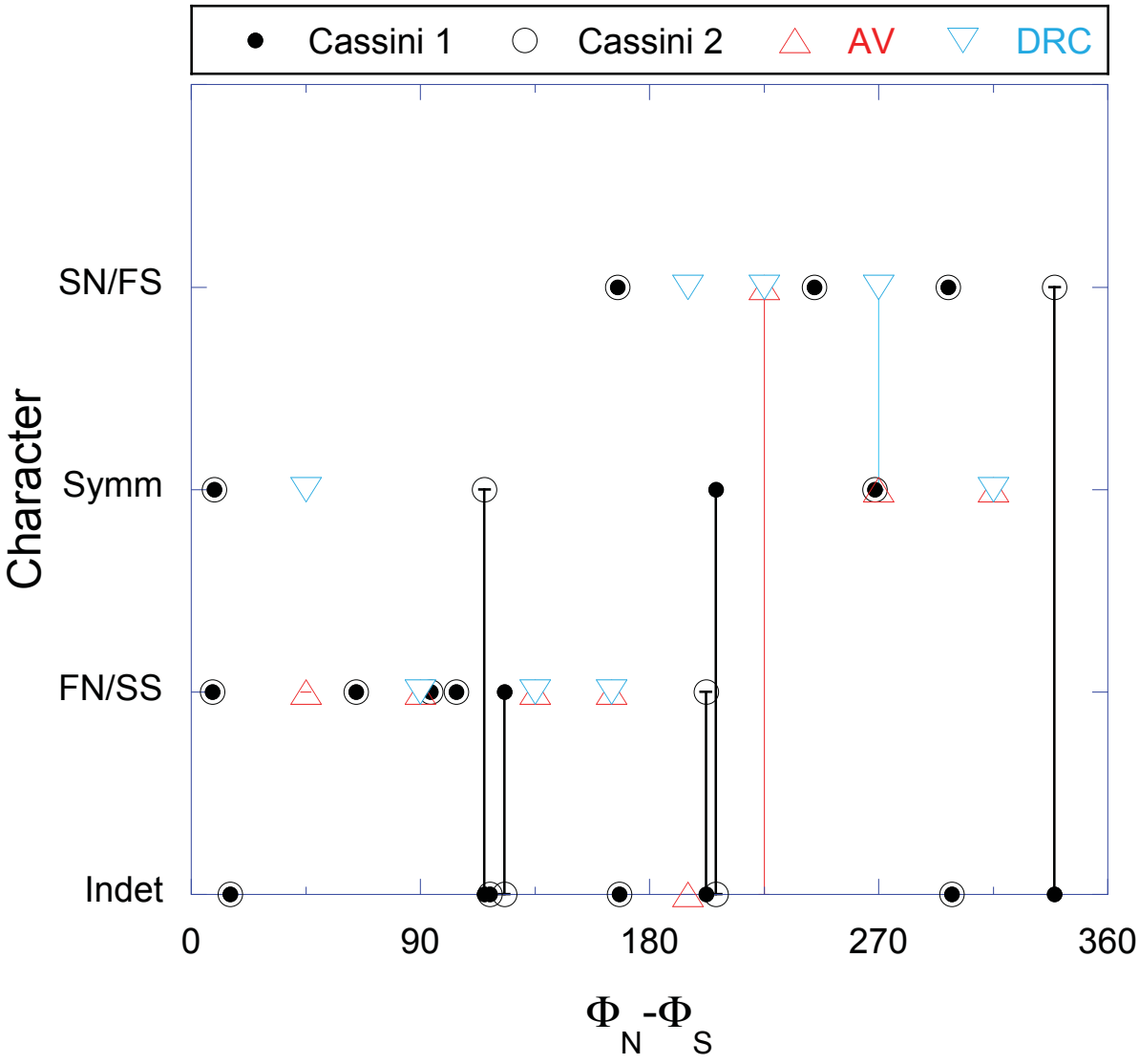
Cassini 1
Cassini 2
AV
DRC
Character
SN/FS
Symm
FN/SS
Indet
0
90
180
270
360
Φ N -Φ S

**Figure 6.**

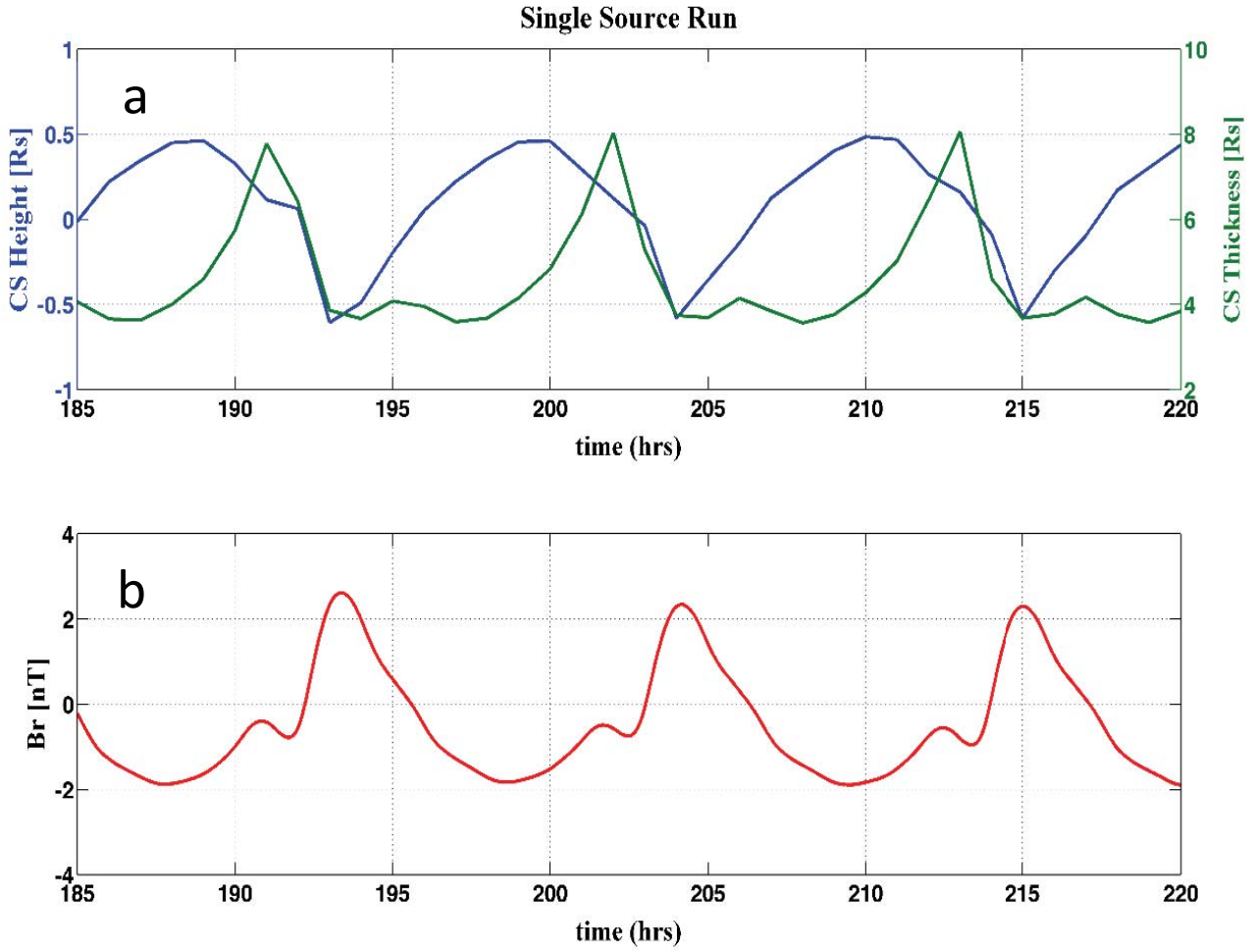
Single Source Run
a
CS Height [Rs]
CS Thickness [Rs]
time (hrs)
b
Br [nT]
time (hrs)